Appl. Magn. Reson. 13, 241–257 (1997)

Applied Magnetic Resonance

A Selective Hole Burning Method Applied to Determine Distances between Paramagnetic Species in Photosystems

H. Hara and A. Kawamori

Faculty of Science, Kwansei Gakuin University, Nishinomiya, Japan

Received July 4, 1996; revised May 16, 1997

Abstract. A method of selective hole burning in EPR spectra was applied to determine the distances from a radical to the acceptor quinone-iron in bacterial and plant photosystems. A low amplitude hole burning 180° pulse and high amplitude 90° and 90° pulses applied to detect ESE of $P870^+$ in *Rb. Sphaeroides* and the distance from the primary electron donor $P870^+$ to the acceptor $Q_A^- Fe^{2+}$ was determined to be 26±2 Å from the dipolar broadening of the burned hole in $P870^+$ EPR. This result is consistent with that given by X-ray analysis and susceptibility measurement. In plant photosystem II the same method was applied to the EPR spectrum of tyrosine D^+, but the effect of crystalline field splitting of Fe^{2+} ion was taken into consideration. The effective spin value for the ferrous iron in PS II was found to be 0.8 and the distance between the radical and the non-heme iron was obtained to be 42±2 Å.

1. Introduction

Two protein subunits, L and M, in the bacterial reaction center (RC) of *Rb. Sphaeroides* R-26 include electron transfer cofactors; four bacterio-chlorophylls, two bacterio-pheophytins, two ubiquinones and one non-heme iron. Two of four bacteriochlorophylls as the primary electron donor (P870) is oxidized by light irradiation, resulting in reduction of the primary acceptor quinone. The oxidized primary electron donor gives rise to a narrow EPR signal of $\Delta H \approx 8.5$ G at $g = 2.0026$ [1] and has been known as a dimer [2]. The reduced primary acceptor has a wide EPR signal centered at $g = 1.8$ [3] due to an exchange interaction with the ferrous iron. The electronic structure of Fe^{2+} in the RC from *Rb. Sphaeroides* was studied in detail [4], where weak exchange interaction between the primary acceptor quinone and the iron with components, $J_x = -0.13$ K, $J_y = -0.58$ K and $J_z = -0.58$ K, is reported. The crystal structure of *Rb. Sphaeroides* has been determined by X-ray diffraction with a resolution of 2.8 Å [5], and the distance from the primary electron donor to the acceptor iron was estimated to be 27 Å [6].

In photosystem II (PS II) there are two 32 kD polypeptides called D1 and D2 located symmetrically about the donor P680. These proteins are believed to bind almost all electron-transfer components of PS II, the Mn-cluster in the oxygen evolving complex, the tyrosine donors D (Y_D) and Z (Y_Z), the primary electron donor P680, two pheophytins, and primary (Q_A) and secondary (Q_B) electron acceptor quinones [7–10]. In PS II there have been no X-ray diffraction data because of difficulty in crystallization of its reaction center. Some structural studies have been attempted by EPR spin-lattice relaxation measurement of the oxidized tyrosine D (Y_D^+) [11–14]. In addition, the structural similarity in the homology between PS II and bacterial RC has been suggested by a computer simulation [10]. In the previous work, we estimated the distance between tyrosine D and the acceptor iron by employing a novel electron spin echo method [15] in a Mn-depleted PS II. The method is based on the selective hole burning in a monitored EPR spectra, and detecting the dipolar interaction between paramagnetic species. The dipolar interaction manifests itself in subsequent hole broadening due to spectral diffusion induced by spin-lattice relaxation of the dipolar coupled spins. The distance obtained by this method is expected to give more correct information than that obtained by spin-lattice relaxation measurements. The previous experiment has shown that the distance from Y_D to the acceptor iron was determined to be 52 Å using the spin number $S = 2$ for $Q_A Fe^{2+}$ states as indicated in a bacterial RC [4] and $S = 3/2$ for $Q_A^- Fe^{2+}$ states for fitting the formula shown in [15]. This result suggested that the exchange interaction between Q_A^- and Fe^{2+} might be rather strong compared to the bacterial equivalent [4]. The distance derived, however, is much larger than 37 Å derived by Hirsh *et al.* [11] from the spin-lattice relaxation time measurement. This discrepancy may be ascribed to some reduction of the effective spin number due to the crystalline field splitting of Fe^{2+}. To elucidate the cause of the discrepancy in PS II in more detail, and to prove the reliability of the hole burning method applied to photosystems, we study the distance between the primary electron donor (P870) and the acceptor iron in *Rb. Sphaeroides* R-26. The result was compared to the available structural data [5, 6]. Because both systems are similar in the acceptor side, we use the electronic states of Fe^{2+} studied for *Rb. Sphaeroides* to derive the approximate distance from Y_D to the quinone iron in PS II.

2. Experimental

2.1. Samples

The RC was suspended in 0.1 M Tris (2-amino-2-hydroxymethylpropane-1,3-diol)-HCl (pH 8.0) buffer with 0.1% triton X-100 [16]. The suspension (≈200 μM RC) with 50 vol.% glycerol added was loaded into Suprasil quartz tubes with the inner diameter of 4 mm and the height of 10 mm and was stored in liquid nitrogen until measurements. Before EPR experiment, the thawed sample at 273 K was incubated in the dark for 1 h and illuminated for 1 min at room temperature by a 500 W tungsten Br_2-light through a 5 cm thick water layer. During illumination, the sample

was transferred into the liquid nitrogen within several seconds. This treatment produces the complete charge separation of RC into $P870^+$ and $Q_A^-Fe^{2+}$.

The oxygen evolving PS II membranes were prepared from spinach using the method of Kuwabara and Murata [17] and light harvesting proteins were removed by the method described in [18]. To deplete manganese from PS II membranes, the oxygen-evolving PS II membranes were treated with 0.8 M Tris buffer [19]. The pellet was washed twice with a suspension buffer, 200 mM sucrose, 20 mM NaCl, 20 mM Mops (4-morpholinopropanesulfonic acid) (pH 6.8). The samples in Chl (chlorophyll) concentration of 6–7 mg of per ml (50 μM RC) with 50 vol.% glycerol added were loaded into Suprasil quartz tubes with and without 50 mM DCMU (3-(3,4-dichlorophenyl)-1,1-dimethylurea). Both samples, in the Q_AFe^{2+} state in the dark, could be transformed to the $Q_A^-Fe^{2+}$ state after preillumination at 273 K for 1 min then dark adapted about 30 min. In the sample without DCMU $Q_A^-Fe^{2+}$ was converted to Q_AFe^{2+} state during the dark adaptation.

2.2. Selective Hole Burning Methods

The experimental technique for the selective hole burning of $P870^+$ in *Rb. Sphaeroides* and Y_D^+ in PS II was the same as that described previously [20, 21]. A pulsed Bruker ESP 380 FT-EPR spectrometer was equipped with a cylindrical dielectric cavity (ER4117 DLQH, Bruker), a helium gas-flow system (CF935, Oxford Instrument) and a 1 kW TWT amplifier (Model 117X Applied System Engineering). One channel of the microwave pulse-former unit of the device was used to form a selective low-amplitude hole-burning pulse (P0). Another channel was used to form nonselective high-amplitude free-induction and echo forming pulses (P1 and P2). The pulse sequence was $180°–T–90°–\tau–90°$ as shown in Fig. 1. The phase for signal detection pulse was adjusted to provide a maximum free induction signal after the P1 pulse. The data acquisition was performed using a LeCroy 9400A 175 MHz oscilloscope that was triggered simultaneously with the P1 pulse. The sampling step was 10 ns. The video amplifier bandwidth was set at 50 MHz. Usually the signal was accumulated 20000 times and then recorded. The free induction decay (FID) following the P1 pulse presents the later part of the effect of the spectral diffusion, while the echo signal shows its early part. Both signals were analyzed complementarily. After the measurement carried out with the P0 pulse turned on as shown in Fig. 1a, the experiment was repeated with the pulse turned off as in Fig. 1b, and then the latter trace was subtracted from the former one. The length of the P0 pulse was 400 ns. The time interval between the P1 and P2 pulses was 800 ns. The P1 and P2 pulse lengths were equal to 32 ns. To eliminate unwanted echoes appearing at small times T, a phase-cycling method was used [15, 20, 21]. The same measurements were performed twice with the phase of the P0 pulse in the second measurement changed by 180° with respect to that in the first measurement, and then recorded traces were added. This phase difference was manually adjusted observing the receiver signal on the oscilloscope.

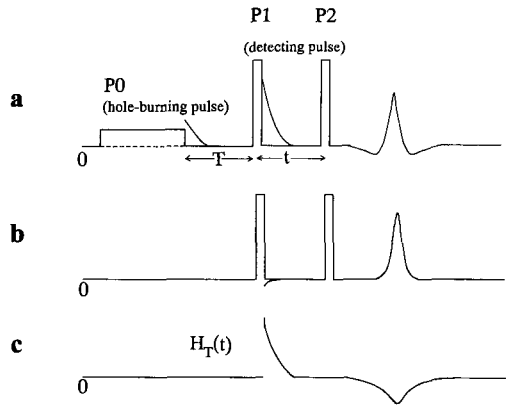

Fig. 1. The pulse sequence (180°–T–90°–τ–90°) for the selective hole burning methods. The low-amplitude P0 pulse burns a selective hole into the EPR spectrum which results in appearance of the strong FID signal following the P1 pulse, and in change of the echo shape (**a**). **b** shows the pattern with the P0 pulse off. **c** shows that subtraction **b** from **a** results in the time profile of the hole shape.

To investigate the spin-lattice relaxation rate of the $Q_A^- Fe^{2+}$ signal of *Rb. Sphaeroides*, the saturation recovery transients were measured. To saturate the magnetization completely, five 90° (16 ns) pulses were applied with the separation of 8 μs. Recovery of the magnetization was monitored by the primary echo amplitude as a function of the time interval t between the end of the saturating pulses train and the beginning of the two echo-forming pulses.

3. Theory

In the beginning, we distinguish two groups of spins, the A spins that are excited by the hole-burning pulse, and the B spins that are not excited but cause a hole broadening of the A spins. In this case, the A spins belong to the primary electron donor $P870^+$ in *Rb. Sphaeroides* or Y_D^+ in PS II and the B spins to the non-heme irons Fe^{2+} on the acceptor side. The interaction between A spins can be ignored because of their small concentration of about 50–200 μM that corresponds to the average space separation more than 100 Å. For simplicity, we take g-factors for both types to be isotropic and the values of spins to be 1/2. For pairwise distribution of spins, the frequency shift of A spins caused by the dipole-dipole interaction with B spins is determined by [22, 23]:

$$\varepsilon(r,\theta) = \gamma_A \mu_B (1 - 3\cos^2\theta)/r^3 , \tag{1}$$

where γ_A is the gyromagnetic ratio of A spins, μ_B is the magnetic moment of B spins ($\mu_B = g_B\beta$ and β is the Bohr magneton), r is the distance between A and B spins, and θ is the angle between the vector $\mathbf{r}$ and the static magnetic field $\mathbf{H}_0$.

The shift of the resonance frequency of the A spin induced by the dipolar interaction with a B spin is determined by the product $\varepsilon(r,\theta)m_B$, where $m_B = \pm 1/2$ are the projections of the B spin onto the axis $z \| \mathbf{H}_0$. When the B spin flips, the resonance frequency of the A spin changes, resulting in spectral diffusion. The frequency shift relative to that at time $t = 0$, will be 0 or $\pm\varepsilon$ (0 means the return to the original value by even times flip-flop) depending on the m_B value at $t = 0$. Thus, if at $t = 0$ the hole shape is described by a function $h_0(\omega)$, then after time $t = T$ the shape will be given by:

$$h_T(\omega) = 0.5\left(1 + \exp(-T/T_1)\right)h_0(\omega) + 0.5\left(1 - \exp(-T/T_1)\right) \times \left[0.5h_0\left(\omega + \varepsilon(r,\theta)\right) + 0.5h_0\left(\omega - \varepsilon(r,\theta)\right)\right] , \quad (2)$$

where T_1 is the spin-lattice relaxation time of B spins, and $\varepsilon(r,\theta)$ is the magnitude of dipolar interaction between A and B spins given by Eq. (1). Here the broadened hole given by Eq. (2) is observable only when the condition $T_1 > 1/\varepsilon(r,\theta)$ is fulfilled. If all A spins are equally excited, the cosine Fourier transformation of the spectrum determines the FID signal of A spins. The condition of equal excitation is fulfilled within the narrow hole burned out by the low-amplitude selective pulse. Then $H_T(t)$ corresponds to the Fourier transformation of the hole depth $1 - h_T(\omega)$:

$$H_T = \int_{-\infty}^{\infty} d\omega (1 - h_T(\omega)) \cos(\omega t) \ . \quad (3)$$

Substituting Eq. (2) into Eq. (3), applying the shift theorem for Fourier transformation [24], we obtain the following function:

$$H_T(t) = H_0(t)\left[0.5\left(1 + \exp(-T/T_1)\right) + 0.5\left(1 - \exp(-T/T_1)\right)\cos(\varepsilon(r,\theta)t)\right] \ . \quad (4)$$

As mentioned above, the data acquisition is performed twice: with the hole-burning pulse (P0) turned on and off. After subtraction of the latter measurement from the former, the resulting FID, $H_T(t)$, refers solely to the hole and can be represented as given in [20, 21]:

$$H_T(t) = H_0(t)f_T(t) \ , \quad (5)$$

where the subscript T refers to the time passed after the hole-burning pulse. The Fourier transform of $H_T(t)$ represents the hole shape in frequency domain. The function $f_T(t)$ describes the hole broadening induced by spectral diffusion. Then taking into account Eqs. (4) and (5), we obtain the following function:

$$f_T(t) = 0.5\left(1 + \exp(-T/T_1)\right) + 0.5\left(1 - \exp(-T/T_1)\right)\cos(\varepsilon(r,\theta)t) \ . \quad (6)$$

For a B spin with $S_B > 1/2$ the formula would be more complicated, because the transitions between several different spin orientations may contribute to the spectral diffusion. Moreover, these transitions may be characterized by the different spin-lattice relaxation times T_1. Therefore, the best way is to perform the measurements, when the condition $T \gg T_1$ holds for all possible transitions. In this case, the time T_1 as a parameter will be excluded from consideration. In the general case of an arbitrary spin number S_B, the function $f_\infty(t)$ for $T \gg T_1$ in all sublevels can be obtained in the same way:

$$f_\infty(t) = \frac{1}{2S+1} + \sum_{k=1}^{2S} \frac{2(2S+1-k)}{(2S+1)^2} \cos(k\varepsilon(r,\theta)t) \quad . \tag{7}$$

For a randomly oriented system, Eq. (7) is to be averaged over the angle θ and the following function can be derived:

$$f_\infty(t) = \frac{1}{2S+1} + \sum_{k=1}^{2S} \frac{2(2S+1-k)}{(2S+1)^2} \int_0^\pi \cos(k(\varepsilon(r,\theta)t) \sin\theta \, \mathrm{d}\theta/2 \quad . \tag{8}$$

In the following Eq. (8) will be applied to systems of B spins of Fe^{2+} with $S = 2$.

4. Results and Discussion

4.1. The Distance between P870 and the Quinone Iron in Rb. Sphaeroides R-26

Figure 2a depicts the experimentally obtained traces, FID and spin echo, for $P870^+$ of *Rb. Sphaeroides* broadened by the dipolar interaction with the $Q_A^- Fe^{2+}$ spin, obtained from measurements at the temperature of 20 K for different times T after the P0 pulse. The result of the measurement without the P0 pulse has been subtracted from that with the P0 pulse. As the echo amplitude decreased by a few percent for large T because of the spin-lattice relaxation of the $P870^+$ radical, all traces were normalized to the same value of the resulting echo amplitude. The FID following the P1 pulse and the echo signal were analyzed. For both signals, the transient trace is to be fitted with the same theoretical function, $H_T(t)$. The possible sources of spectral diffusion of the $P870^+$ EPR signal are the dipolar interactions with the Fe^{2+} ion on the acceptor side of the *Rb. Sphaeroides* RC. The experimental traces obtained for $T = 180$ and 260 μs are different. This shows that T_1 of the B spin is rather long and the condition $T_1 \ll T$ is not fulfilled. However, in Fig. 2b that shows the result obtained at the temperature of 40 K, the traces of $H_T(t)$ for $T = 180$ and 260 μs are almost identical. Thus the condition $T_1 \ll T$ is fulfilled for $T = 260$ μs at this temperature. Figure 3 enlarges time scale of the experimentally obtained functions $f_T(t)$

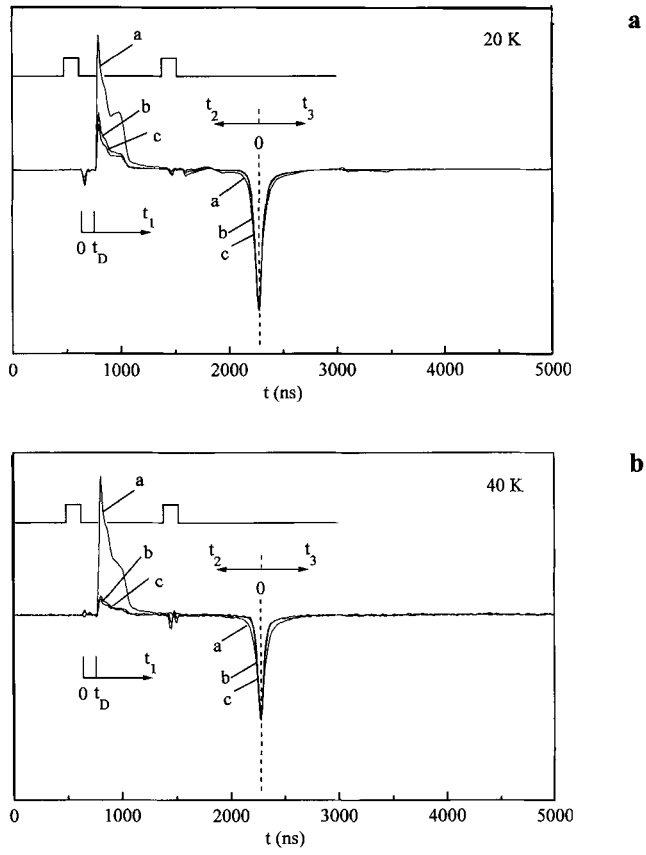

Fig. 2. The resultant FIDs and echo shapes $H_T(t)$ recorded at 20 K (**a**) and 40 K (**b**) for *Rb. Sphaeroides* R-26 in the $Q_A^-Fe^{2+}$ state, obtained by difference of the traces with the P0 pulse turned on and off. The echo amplitudes $H_T(0)$ are adjusted to give the same amplitude. The traces a, b and c correspond to T = 2, 180, and 260 μs, respectively. The traces are to be analyzed as a function of time t; three time dependencies $H_T(t_1)$, $H_T(t_2)$ and $H_T(t_3)$ should be same. t_D is the dead time.

from measurements at the temperature of 20 and 40 K. To obtain $f_T(t)$, it is necessary to divide the function $H_T(t)$ by the function $H_0(t)$ acquired at the smallest value of time T (2 μs in this work) according to Eq. (6). As mentioned above, the experimental results for T = 180 and 260 μs are different at 20 K but almost identical at 40 K. This shows that we can apply Eq. (8) to analyze the experimental data.

To investigate the relation between obtained traces $f_T(t)$ and the spin-lattice relaxation time T_1 of $Q_A^-Fe^{2+}$, magnetization recovery of $Q_A^-Fe^{2+}$ signal was measured. Figure 4 shows the saturation recovery transients obtained at g = 1.8 magnetic field position after several saturation pulses for three different temperatures. One can see that the $Q_A^-Fe^{2+}$ magnetization has a clear non-exponential relaxation kinetics at 4.2 and 20 K and does not completely recover after 180 μs.

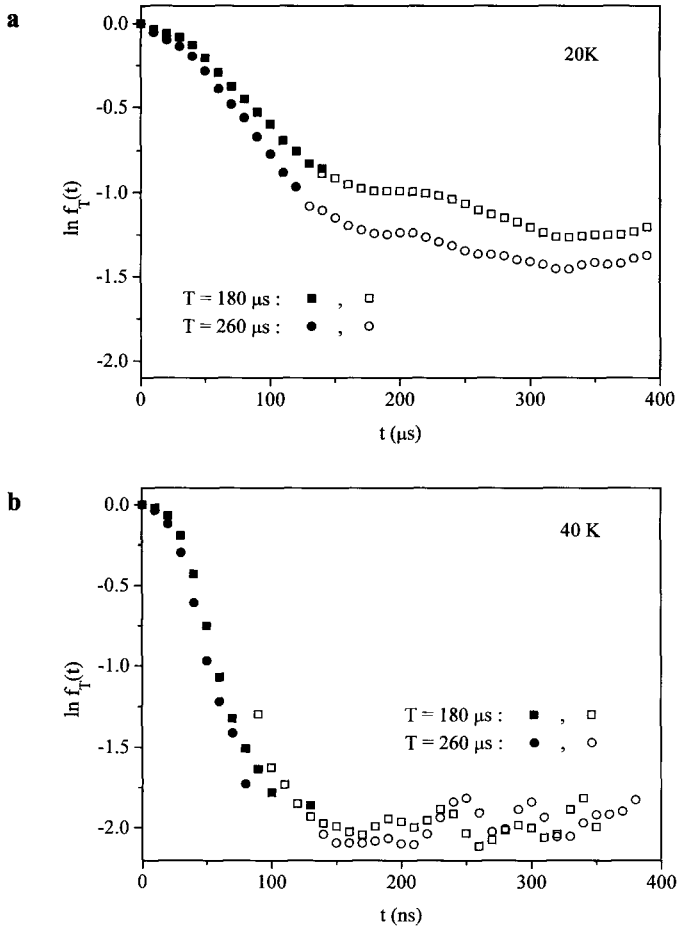

Fig. 3. The function $f_T(t)$ obtained at 20 K (**a**) and 40 K (**b**) for *Rb. Sphaeroides* in the $Q_A^- Fe^{2+}$ states. Squares and circles indicate the results for T = 180 and 260 μs, respectively. Closed squares and circles are obtained from the echo shape and open symbols from the FID.

These non-exponential relaxation kinetics can be fitted with a double-exponential function. The spin-lattice relaxation rate at 20 K were composed of two parts with $T_{1,slow}$ = 29 μs and $T_{1,fast}$ = 4.4 μs, respectively. The slow relaxation kinetics results in the difference between traces of T = 180 and 260 μs at 20 K as shown in Figs. 2a and 3a. Figure 5 shows the temperature dependence of $1/T_{1,slow}$ and $1/T_{1,fast}$ derived from the saturation recovery transients measured at the field of g = 1.8 position. As the temperature decreases, both relaxation rates become slow. As the spin exchange between the quinone and the iron is fast [4], these complex rates may be ascribed to the spin-lattice relaxation rates of the ferrous iron. Note that in our system, there are no other radicals which might enhance the spin-lattice relaxation rate. Both relaxation kinetics can be explained by an Orbach

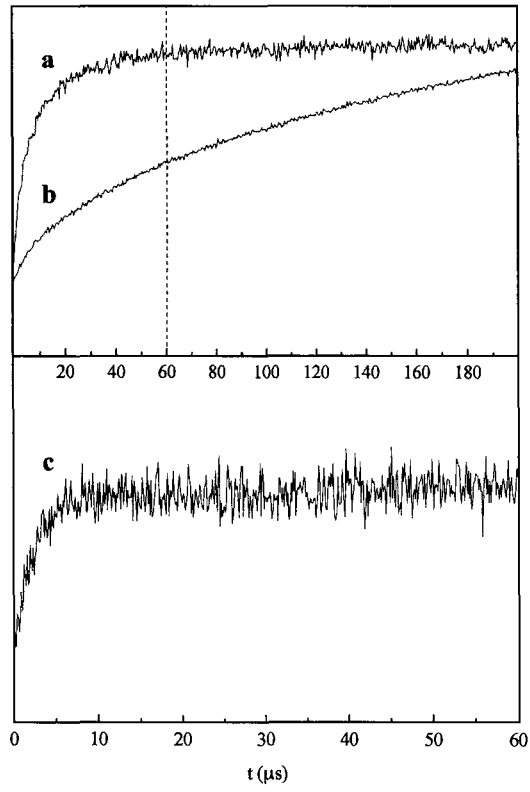

Fig. 4. Saturation recovery transients measured at 4.2 K (**a**), 20 K (**b**) and 40 K (**c**) at the magnetic field fixed at the position of $g = 1.8$. The curves are fitted with the function $A\exp(-at) + + (1 - A)\exp(-bt)$, a and b are the fast and slow spin-lattice relaxation rates, respectively.

process [25] and fitted with $T_1 \propto \exp(34/T_e)$ above 15 K and $T_1 \propto \exp(3/T_e)$ below 15 K, where T_e is a temperature. The susceptibility measurement has shown that the first excited doublet lie approximately 3 K above the ground doublet and the third doublet, approximately 33 K above the ground doublet [4]. This is in good agreement with our experimental result of T_1 measurements.

Figure 6 shows the experimental results of $f_T(t)$ observed for $T = 260$ μs at temperatures 4.2, 20, and 40 K. The trace c measured at 40 K is satisfied by the condition $T_1 \ll T$ and we can apply Eq. (8) to it. However, traces a and b obtained at 4.2 and 20 K, respectively, are not satisfied by the condition $T_1 \ll T$, and the effect of spin-lattice relaxation must be taken into consideration in traces a and b. In the simulation by Eq. (8), we are going to use a point dipole approximation for the $P870^+$ and $Q_A^-Fe^{2+}$ pair. The best fit value of the distance for the trace c was estimated to be 27±2 Å, assuming the spin number 2 as shown by the calculated curve based on Eq. (8). This result agrees well with the value of 27 Å for the distance between $P870^+$ to the iron previously determined by X-ray

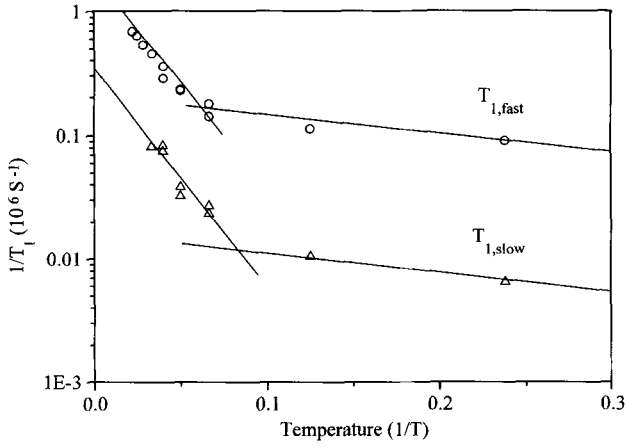

Fig. 5. Temperature dependence of saturation recovery transients. Circles and triangles show the fast and slow relaxation kinetics, respectively. The solid lines are drawn by $\exp(-34/T_c)$ above 15 K and by $\exp(-3/T_c)$ below 15 K.

analysis [5, 6]. The spin number 2 assumed in this simulation shows the exchange interaction between the ferrous ion and the acceptor quinone is small enough to neglect the effect of the existence of the radical Q_A^- with the spin 1/2 in *Rb. Sphaeroides*. The magnetic exchange interaction tensor components between Q_A^- and the ferrous ion derived were $J_x = -0.13$ K, $J_y = -0.58$ K and $J_z = -0.58$ K [4], which rationalize this assumption. Furthermore the effect of crystalline field

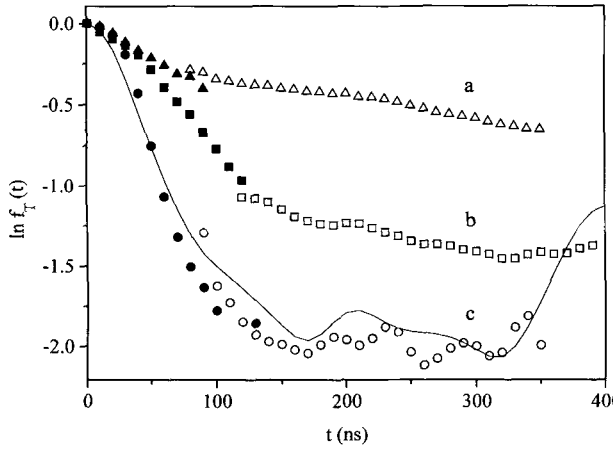

Fig. 6. Observed function $f_T(t)$ obtained at the temperature 4.2 K (a), 20 K (b) and 40 K (c) for *Rb. Sphaeroides* in the $Q_A^-Fe^{2+}$ state for $T = 260$ μs. Closed symbols are obtained from the echo shape, and open symbols from the FID. Solid line is the best fit value calculated by Eq. (8) for $S = 2$ and $r = 27$ Å.

splitting with $D = 7.94$ K and $E = 2.11$ K [4], also can be neglected at 40 K in *Rb. Sphaeroides*, because all spin states are occupied.

4.2. The Distance between Tyrosine D and the Quinone Iron in PS II

In order to apply the same analytical method to PS II as in *Rb. Sphaeroides*, we measured Y_D^+ EPR for two different states of Mn-depleted PS II: Q_AFe^{2+}, $Q_A^-Fe^{2+}$, respectively, on the acceptor side. Figure 7 shows the experimental result of $f_T(t)$

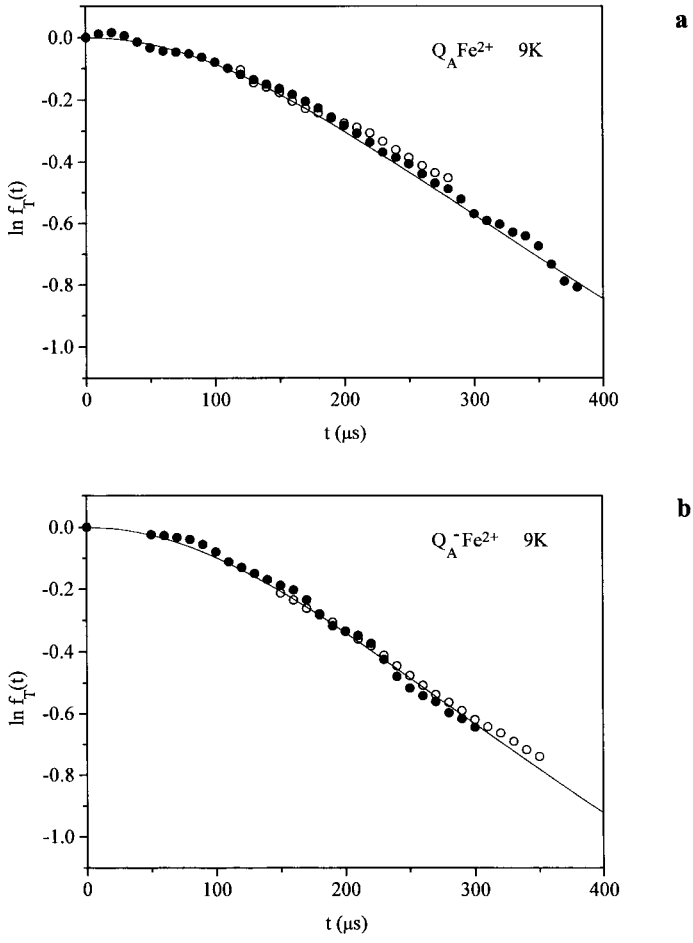

Fig. 7. The -function $f_T(t)$ obtained at 9 K for Mn-depleted PS II in the Q_AFe^{2+} state (**a**) and the $Q_A^-Fe^{2+}$ (**b**). Circles indicate the results for $T = 260$ μs. Closed circles are obtained from the echo shape and open circles, from the FID shape. Solid lines are the best fit values calculated by Eq. (8) for $S = 2$, $r = 53$ Å for Q_AFe^{2+} and $r = 52$ Å for $Q_A^-Fe^{2+}$, respectively. Same values can be obtained by Eq. (18) for $S = 2$, $r = 43$ Å for Q_AFe^{2+} and $r = 42$ Å for $Q_A^-Fe^{2+}$ with $D = 7.94$ K, $E = 2.11$ K and $T_e = 9$ K.

obtained at 9 K for Mn-depleted PS II in the Q_AFe^{2+} and $Q_A^-Fe^{2+}$ states. The maximum decrease in echo amplitude due to the hole broadening was observed at 9 K. At this temperature, the experimental results for 180 and 260 μs are almost identical, and the condition $T_1 \ll T$ is satisfied for $T = 260$ μs. The lines drawn through experimental points in Fig. 7 are obtained using Eq. (8) and assuming $S = 2$ for both states. The best fit value of the distances is estimated to be 53±2 Å for the Q_AFe^{2+} state and 52±2 Å for the $Q_A^-Fe^{2+}$ state. After all, we could obtain almost the same distances for these two states of PS II. In previous report [15], we applied the value of spin $S = 3/2$ for $Q_A^-Fe^{2+}$ state as the best fit value. This differs from the present result. Probably this difference is ascribed to an experimental error caused by a temperature fluctuation. If we apply the spin number $S = 3/2$ for $Q_A^-Fe^{2+}$ state, the distance was estimated to be 49 Å. Though this value is smaller than the value obtained above and seems to be reasonable, the exchange interaction between Q_A^- and Fe^{2+} is considered to be also weak as in *Rb. Sphaeroides* R-26 [4] and the presence of the reduced acceptor quinone radical may not change the distance. However, the value of 52 Å seems to be too large compared to the value of 37 Å derived from spin-lattice relaxation rate and also to the suggested value by Svensson *et al.* [10].

To determine the distance from the trace $f_T(t)$ for $T \gg T_1$, we have to consider only two parameters: r, the distance and S, the spin number. On the other hand, if the spin-lattice relaxation time for B spin becomes shorter than the time resolution limit $T = 2$ μs, the broadening due to spectral diffusion induced by this fast relaxation might occur before the time 2 μs and the effect of spectral diffusion is hard to observe. For this reason the simulation assumes appropriate T_1 values. The appropriate value of spin-lattice relaxation time 260 μs $\gg T_1 >$ 2 μs can be found by measuring the temperature dependence of $f_T(t)$ of $Q_A^-Fe^{2+}$. In Mn-depleted PS II samples, in fact, the $f_T(t)$ functions vary remarkably with temperature and the maximum effect of spectral diffusion was found at 9 K for both $Q_A^-Fe^{2+}$ and Q_AFe^{2+} states. Contrary to our previous experiment, we have to assume the spin value for $Q_A^-Fe^{2+}$ to be same as for Q_AFe^{2+} in this experiment. This result indicates that the exchange interaction between the plastoquinone and the ferrous ion is also small as in *Rb. Sphaeroides*. Comparing the results with those in $f_T(t)$, there is one remarkable difference in the optimum temperature, where the effect of spectral diffusion is most effective ($T \gg T_1$). It is 40 K for $f_T(t)$, while 9 K for the PS II. This indicates that the spin-lattice relaxation time of the acceptor quinone in the Mn-depleted PS II is shorter than that in *Rb. Sphaeroides* below 40 K. Furthermore the spin relaxation time T_2 of $Q_A^-Fe^{2+}$ EPR signal may be also short, because we cannot observe the signal in the Mn-depleted PS II by pulsed EPR but can observe it by CW-EPR at a rather strong microwave power of 80 mW at 6 K [26]. However, the values of T_1 seems to be longer than 2 μs corresponding to the condition for Eq. (2), $T_1\varepsilon(r,\theta) > 1$, because we could indeed observe the maximum hole broadening effect at 9 K.

On the other hand, the effect of the crystalline field splitting [4] should be taken into consideration at the low temperature of 9 K, if its magnitude is compara-

tive to the measurement temperature. The spin Hamiltonian for Fe^{2+} ($S = 2$) is usually given by in a crystalline coordinate system (X, Y, Z):

$$\mathcal{H} = g\beta \mathbf{H}_0 \cdot \mathbf{S} + D[S_Z^2 - S(S+1)/3)] + E(S_X^2 - S_Y^2) \ , \tag{9}$$

where D and E are zero field splitting constants. It will be more convenient to describe the spin Hamiltonian in terms of the laboratory frame (x, y, z), in which Y_D^+ spin orientation is quantized along the static field direction ($\mathbf{H}_0 \| z$):

$$\mathcal{H}(\mathbf{\Omega}) = g\beta H_0 S_z + D[S_3^2 - S(S+1)/3)] + E(S_1^2 - S_2^2) \ , \tag{10}$$

where $S_{1,2,3}$ are the spin components of $S_{X,Y,Z}$ in the laboratory frame. $\mathbf{\Omega} = \mathbf{\Omega}_1 \cdot \mathbf{\Omega}_2$, $\mathbf{\Omega}_1(\alpha,\beta,\gamma)$ and $\mathbf{\Omega}_2(\varphi,\theta,\psi)$, are Eulerian angle matrixes which define the orientations of the crystalline field of the non-heme iron and the distance vector $\mathbf{r}$ from tyrosine D to the Fe^{2+} ion, respectively, in the laboratory frame. The spin operators S_x, S_y and S_z were transformed by the Eulerian angle matrix, $\mathbf{S}(1,2,3) = \mathbf{\Omega} \cdot \mathbf{S}(x,y,z)$, as given by:

$$\begin{aligned} S_1 &= b_{1x}S_x + b_{1y}S_y + b_{1z}S_z \ , \\ S_2 &= b_{2x}S_x + b_{2y}S_y + b_{2z}S_z \ , \\ S_3 &= b_{3x}S_x + b_{3y}S_y + b_{3z}S_z \ , \end{aligned} \tag{11}$$

where, b_{ij}'s ($i = 1$–3, $j = x,y,z$) are direction cosines of the crystalline field axis in the laboratory frame.

Now, the five spin substates m_k, $|2\rangle$ to $|-2\rangle$ belonging to $S = 2$ are chosen as basic spin states. According to Eq. (10) we can find the eigen values E_i and functions Ψ_i ($i = 1$–5), which are mixtures of the five spin quantum states as given by:

$$\mathcal{H}(\mathbf{\Omega})\Psi_i = E_i(\mathbf{\Omega})\Psi_i \ , \tag{12}$$

where $$\Psi_i = \sum_k C_{ik}|m_k\rangle = C_{i1}|2\rangle + C_{i2}|1\rangle + C_{i3}|0\rangle + C_{i4}|-1\rangle + C_{i5}|-2\rangle \ ,$$

$$m_k = -2, \ -1, \ 0, \ 1, \ 2 \ , \qquad i = 1\text{–}5 \ .$$

C_{i1} to C_{i5} are normalized mixing coefficients of the five spin states given by functions of H_0 and $\mathbf{\Omega}$. For each eigen states Ψ_i the occupation ratio P_i was defined by Boltzmann distribution:

$$P_i(H_0, \mathbf{\Omega}, T_e) = \frac{\exp(-E_i/kT)}{\sum_i \exp(-E_i/kT)} \ , \tag{13}$$

where E_i is the i-th energy, T_e is the temperature and k is the Boltzmann constant. The z-component of the dipolar field H_{Dz} effective for the broadening of a

burned hole in Y_D^+ EPR, includes not only S_{Bz} but also S_{Bx} and S_{By} of the Fe^{2+}, because the latter two have diagonal matrix elements in the laboratory frame:

$$H_{Dz} = D_{zx}S_{Bx} + D_{zy}S_{By} + D_{zz}S_{Bz} \ , \tag{14}$$

D_{ij}'s ($i = z$, $j = x,y,z$) are the dipolar interaction tensors and are given by:

$$\begin{aligned} D_{zx} &= -3\gamma_A\mu_B\cos\theta\sin\theta\cos\varphi/r^3 \ , \\ D_{zy} &= -3\gamma_A\mu_B\cos\theta\sin\theta\sin\varphi/r^3 \ , \\ D_{zz} &= \gamma_A\mu_B(1 - 3\cos^2\theta)/r^3 \ , \end{aligned}$$

where $\mu_B = g_B\beta$ (g_B is the g-factor for the non-heme iron), and θ and φ define the direction of the vector $\mathbf{r}$ in the laboratory frame.

To calculate the hole broadening effect, let us assume the time T applied after the hole burning pulse for Y_D^+ EPR line is longer enough than the spin-lattice relaxation time for all five energy levels. The frequency, ω_i, corresponding to the local magnetic field at Y_D^+ site induced by the dipolar field due to the i-th state of the non-heme iron (Fe^{2+}) is defined by:

$$\omega_i = \langle \Psi_i|H_{Dz}|\Psi_i\rangle = D_{zx}\langle \Psi_i|S_{Bx}|\Psi_i\rangle + D_{zy}\langle \Psi_i|S_{By}|\Psi_i\rangle + D_{zz}\langle \Psi_i|S_{Bz}|\Psi_i\rangle \ , \tag{15}$$

where $i = 1$–5. For the initial state at $T = 0$, there are five probable spin states of the Fe^{2+} given by Eq. (13). After $T \gg T_1$, the final five spin states for $j = 1$–5 are also distributed in the same way. Then the hole shape at time T can be given in a similar way as Eq. (2):

$$h_\infty(\omega) = \sum_{i=1}^{5}\sum_{j=1}^{5} P_i(H_0,\mathbf{\Omega},T_e)P_j(H_0,\mathbf{\Omega},T_e)\, h_0(\omega_0 + \Delta\omega_{ij}) \ , \tag{16}$$

where $\Delta\omega_{ij}$'s are the frequency shifts at Y_D^+, from the initial state i to the final state j defined as $\Delta\omega_{ij} = \omega_j - \omega_i$. Applying the similar consideration presented by Eqs. (3)–(6), the hole broadening is described in the time domain by the following form:

$$f_\infty(\omega) = \sum_{i=1}^{5}\sum_{j=1}^{5} P_i(H_0,\mathbf{\Omega},T_e)P_j(H_0,\mathbf{\Omega},T_e)\cos(\Delta\omega_{ij}t) \ . \tag{17}$$

Finally, this function should be averaged over $\mathbf{\Omega}_2(\varphi,\theta,\psi)$ for the orientation of the vector $\mathbf{r}$ and given by:

$$f_\infty(\omega) = \frac{\int \sum_{i=1}^{5}\sum_{j=1}^{5} P_i(H_0,\mathbf{\Omega},T_e)P_j(H_0,\mathbf{\Omega},T_e)\cos(\Delta\omega_{ij}t)\sin\theta\, d\mathbf{\Omega}_2}{\int \sin\theta\, d\mathbf{\Omega}_2} \ . \tag{18}$$

Applying Eq. (18) to the acceptor iron in Mn-depleted PS II at 9 K and using the zero field splitting constants, $D = 7.94$ K and $E = 2.11$ K [4] reported for *Rb. Sphaeroides*, the effective spin value was found to be about 0.8. As there is no data for Ω_1, the crystalline field direction of the Fe^{2+} in PS II, the calculations were carried out on several assumed directions. The result has shown that the value of Eq. (18) only slightly depends on the assumed values for Ω_1. The range of the calculated values was incorporated in the error of distance estimate. Then the distance between Y_D^+ and the Fe^{2+} was estimated to be 42±2 Å for Q_AFe^{2+} state. This results approaches to the distance 37±2 Å derived by Hirsh *et al.* [11]. Though at present there is no data to judge about the correct distance, the value seems to be a little larger than that suggested by Svensson *et al.* [10]. However, the actual distance may differ from this value, because the D and E values of PS II may be different from those in *Rb. Sphaeroides*.

Another possibility is considered that the value used for time $T \approx 0$ (2 μs in this case) is not small enough because of fast spin-lattice relaxation rates. Indeed we have shown the two spin-lattice relaxation rates for the non-heme iron in *Rb. Sphaeroides*. If $T_{1,\text{fast}}$ at 9 K in PS II is shorter than 2 μs, the effect of spectral diffusion might be reduced, which might result in an overestimated distance in PS II. Then further decrease in the distance estimate would be expected. This may be one of the reasons that the obtained distance 42 Å is larger than 37 Å derived by Hirsh *et al.* [11], where they assumed the value of correlation time of Fe^{2+} to be same as in *Rb. Sphaeroides* RC. In another experiment with "2 + 1" sequence ESE method [28], we determined the distance between tyrosine D and Q_A is to be 38 Å [29]. Then the distance between tyrosine D and Fe^{2+} is suggested to be close to this value.

Equation (18) can be also applied to $P870^+$ for *Rb. Sphaeroides*. However, the zero field splitting effect is rather negligible, because the measurement was carried out at 40 K. The distance between the primary electron donor and the acceptor iron is modified only a little to be 26±2 Å, if the value of $S_{\text{eff}} = 1.8$ obtained by Eq. (18) is applied. Thus the correction was not necessary at 40 K based on consideration of the low resolution about 3 Å in structural analysis [5, 6].

Table 1 shows the spin numbers and distances obtained for *Rb. Sphaeroides* and PS II with and without correction for crystalline field splittings. The effective

Table 1. The spin numbers and distances obtained for *Rb. Sphaeroides* R-26 and Photosystem II without and with correction for zero field splitting.

	R-26 (40 K)	PS II (9 K)	
	$Q_A^-Fe^{2+}$	Q_AFe^{2+}	$Q_A^-Fe^{2+}$
Spin number	2	2	2
Distance (Å)	27±2	53±2	52±2
Effective spin number	1.78	0.81	0.81
Corrected distance (Å)	26±2	43±2	42±2

spin numbers and corrected distances were calculated by Eq. (18). We could only derive an approximate distance for PS II because of the limitation of fast spin-lattice relaxation time. A recent preliminary magnetic susceptibility measurement of PS II (unpublished) has shown that the zero field splitting parameter D is approximately the same as that for *Rb. Sphaeroides*, justifying the value of the effective spin number of Fe^{2+} in PS II. Though the value of distance from tyrosine D^+ to $Q_A^-Fe^{2+}$ seems to be a little smaller than that to Q_AFe^{2+}, this difference is comparable to the experimental error. Almost the same distances have been derived, indicating that the weak exchange coupling is not effective to the hole broadening at the temperature 9 K. Therefore two broadening mechanisms due to Q_A^- and Fe^{2+} worked independently and additively on the hole of the tyrosine D^+ EPR. Furthermore the effect of free radical Q_A^- is much less than that of the non-heme iron partly because of the smaller spin value.

5. Conclusion

The selective hole burning method can be applied satisfactorily to determine a radical distance from a transition metal ion, if its spin number is well-defined and spin-lattice relaxation times between each levels are within the range of $1/\varepsilon(r,\theta) < T_1 \ll T$. T is a time to observe the spin echo after the hole burning pulse. By temperature variation we could find the optimal condition and the correct spin number for Fe^{2+} in *Rb. Sphaeroides* RC. For Fe^{2+} in PS II, the condition $1/\varepsilon(r,\theta) < T_1$ might be partly destroyed even at the optimal temperature of 9 K. However, we could get information of the spin-lattice relaxation rate of B spins through finding the optimum condition to detect spectral diffusion, though its EPR signal could not be observed. The spin number at 9 K was derived from the consideration of Boltzmann distribution over the zero field split levels. The derived distance for Y_D^+-Fe^{2+} in PS II from this experiment approaches to the probable distance [29]. The hole broadening of ESE of tyrosine D^+ radical by the ferrous ion is more effective than by the quinone radical in PS II. The accuracy for the obtained distance may be generally comparable to that in a spin-lattice relaxation time measurement, in which we usually look for an optimal temperature to find $\tau_c = 1/\omega_0$.

Acknowledgements

The authors are indebted to Prof. Y. Koyama and Dr. E. Nishizawa in Kwansei Gakuin University for providing the purified RC of *Rb. Sphaeroides* R-26, and to Prof. K. Akabori in Hiroshima University for providing the PS II particles with high concentration. The authors owe Prof. K. M. Salikhov in Kazan Physical-Technical Institute for the discussion in this work. Special thanks to Prof. S. A. Dzuba in Institute Chemical Kinetics and Combustion for his critical reading of the manuscript and valuable discussion. This work was supported partly by a special private fund from Kwansei Gakuin University.

References

[1] Sogo P., Jost M., Calvin M.: Radiat. Res. **1** (Suppl.), 511 (1959)
[2] Norris J.R., Druyan M.E., Katz J.J.: J. Am. Chem. Soc. **95**, 1680 (1973)
[3] McElroy J.D.: Ph.D. Thesis. University of Califolnia, San Diego, La Jolla CA 1970.
[4] Butler W.F., Calvo R., Fredkin D.R., Isaacson R.A., Okamura M.Y., Feher G.: Biophys. J. **45**, 947 (1984)
[5] Allen J.P., Feher G., Yeates T.O., Komiya H., Rees D.C.: Proc. Natl. Acad. Sci. USA **84**, 5730 (1987)
[6] Yeates T.O., Komiya H., Rees D.C., Allen J.P., Feher G.: Proc. Natl. Acad. Sci. USA **84**, 6438 (1987)
[7] Debus R.J., Barry B.A., Babcock G.T., McIntosh L.: Proc. Natl. Acad. Sci. USA **85**, 427 (1988)
[8] Vermaas W.F.J., Rutherford A.W., Hansson O.: Proc. Natl. Acad. Sci. USA **85**, 8477 (1988)
[9] Ruffle S.V., Donnelly D., Blundell T.L., Nungent J.H.A.: Photosyn. Res. **34**, 287 (1992)
[10] Svensson B., Vass I., Cedergren E., Styring S.: EMBO J. **7**, 2051 (1991)
[11] Hirsh D.J., Brudvig G.W.: J. Phys. Chem. **97**, 13216 (1993)
[12] Evelo R.G., Styring S., Rutherford A.W., Hoff A.J.: Biochim. Biophys. Acta **973**, 428 (1989)
[13] Kodera Y., Takura K., Kawamori A.: Biochim. Biophys. Acta **1101**, 23 (1992)
[14] Koulougliotis D., Tang Xiao-Song, Diner B.A., Brudvig G.W.: Biochemistry **34**, 2850 (1995)
[15] Kodera Y., Dzuba S.A., Hara H., Kawamori A.: Biochim. Biophys. Acta **1186**, 91 (1994)
[16] Okamura M.Y., Isaacson R.A., Feher G.: Proc. Natl. Acad. Sci. USA **72**, 3491 (1975)
[17] Kuwabara T., Murata N.: Plant Cell Physiol. **23**, 533 (1982)
[18] Ghanotakis D.F., Demetriou D.M., Yocum C.F.: Biochim. Biophys. Acta **891**, 15 (1987)
[19] Murata N., Miyao M.A., Kuwabara T.: Oxygen Evolving System of Photosynthesis, p. 213. Tokyo: Academic Press 1983.
[20] Dzuba S.A., Kodera Y., Hara H., Kawamori A.: J. Magn. Reson. A **102**, 257 (1993)
[21] Dzuba S.A., Kodera Y., Hara H., Kawamori A.: Appl. Magn. Reson. **6**, 391 (1994)
[22] Salikhov K.M., Tsvetkov Yu.D.: Time Domain Electron Spin Resonance (Kevan L., Schwarz R.N., eds.), p. 231. New York: Wiley 1979.
[23] Raitsimring A.M., Salikhov K.M.: Bull. Magn. Reson. **7**, 184 (1985)
[24] Ernst R.R., Bodenhausen G., Wokaun A.: Principles of Nuclear Magnetic Resonance in One and Two Dimensions, ch. 4. Oxford: Clarendon Press 1987.
[25] Manenkov A.A., Orbach R.: Spin-Lattice Relaxation in Ionic Solids. Charper and Row Pub 1966.
[26] Nugent J.H.A., Diner B.A., Evans M.C.W.: FEBS Lett. **124**, 241 (1981)
[27] Deligiannakis Y., Petrouleas V., Diner B.A.: Biochim. Biophys. Acta **1188**, 260 (1994)
[28] Astashkin A.V., Kodera Y., Kawamori A.: Biochim. Biophys. Acta **1187**, 89 (1994)
[29] Kawamori A., Hara H., Shigemori K., Astashkin A.V. in: Proceedings of 1st Asia-Pacific EPR/ESR Symposium. Hong Kong 1997. Singapore: Springer 1997. (in press)

Author's address: Prof. Asako Kawamori, Faculty of Science, Kwansei Gakuin University, Uegahara 1-1-155, Nishinomiya 662, Japan